This item is the archived peer-reviewed author-version of:

Three-dimensional atomic imaging of colloidal core-shell nanocrystals

Reference:

3D atomic imaging of colloidal core-shell nanocrystals.

Sara Bals[1], Marianna Casavola[2], Marijn A. van Huis[1,3], Sandra Van Aert[1], K. Joost Batenburg[4,5], Gustaaf Van Tendeloo[1], and Daniël Vanmaekelbergh[2]*

[1] EMAT, University of Antwerp, Groenenborgerlaan 171, B-2020 Antwerp, Belgium

[2] Condensed Matter and Interfaces, Debye Institute for Nanomaterials Science, Utrecht University, P.O. Box 80000, 3508 TA Utrecht, The Netherlands

[3] Kavli Institute of Nanoscience, Delft University of Technology, Lorentzweg 1, 2628 CJ Delft, The Netherlands

[4] Vision Lab, University of Antwerp, Universiteitsplein 1, B-2610 Wilrijk, Belgium

[5] Centrum Wiskunde & Informatica, NL-1098XG Amsterdam, The Netherlands

Sara.Bals@ua.ac.be

[*] Corresponding author: email: Sara.Bals@ua.ac.be; Tel: +3232653284; Fax: +3232653318

ABSTRACT

Colloidal core-shell semiconductor nanocrystals form an important class of opto-electronic materials, in which the exciton wave functions can be tailored by the atomic configuration of the core, the interfacial layers and the shell. Here, we provide a trustful 3D characterization at the atomic scale of a free-standing PbSe(core)-CdSe(shell) nanocrystal by combining electron microscopy and discrete tomography. Our results yield unique insights for understanding the process of cation-exchange, which is widely employed in the synthesis of core-shell nanocrystals. The study that we present is generally applicable to the broad range of colloidal hetero-nanocrystals that currently emerge as a new class of materials with technological importance.

KEYWORDS

Colloidal semiconductor nanocrystals with a core-shell geometry form an important class of opto-electronic materials that can be achieved by bottom-up chemical synthesis. The expertise acquired in recent years has shown that the optical properties of such systems, largely determined by the exciton wave functions, can be tailored by the atomic configuration of the core, the interfacial layers and the shell[1-4]. For instance, suitable combinations of core and shell semiconductors have resulted in core-shell systems with striking and very useful optical properties, such as non-blinking systems with unity photoluminescence quantum yield[5,6]. Shells of a second semiconductor compound around a semiconductor core were originally designed in order to passivate the electronic surface states of the core and increase the (photochemical) stability of colloidal nanocrystals. As a result, stable and highly luminescent core-shell systems are available in which Auger non-radiative recombination is suppressed[5,6], holding promise for biological research[7], large-scale illumination, photocatalysis[8], LEDs[9], and LASERs[10]. Core-shell particles have also been designed with the purpose of band edge staggering[11-14]; such systems show strongly reduced recombination rates for the single and bi-excitonic states[15,16] and energy shifts, resulting in e.g. photocatalytic activity[8] and a considerable reduction of the laser threshold[17]. In recent years, it became gradually clear that the electronic structure of core-shell and other hetero-nanocrystals is determined by the details of the atomic landscape, i.e. the presence or absence of atomic mixing, interfacial strain and strain-induced defects[5,6,18-20]. Further progress in opto-electrical engineering will therefore depend on a quantitative characterization and thorough understanding of the structure at the atomic scale with special focus on the interfaces. High resolution transmission electron microscopy (HRTEM) is the standard technique to investigate the atomic structure of (nano)crystals. However, HRTEM only provides a two dimensional (2D) projected image and it is not straightforward to extract quantitative three dimensional (3D) information. Hence, it is very difficult to obtain the complete atomic structure of an individual core-shell nanocrystal including all its interfaces. In contrast, high angle annular dark field - scanning transmission electron microscopy (HAADF-STEM) enables one to obtain projections of the (interfacial) atomic columns in core-shell nanocrystals that can be

interpreted in a quantitative manner and very recently, a novel technique to extract 3D information from 2D data has been proposed[21]. However, this technique was only applied for metal nanocrystals embedded in a stabilizing matrix with the same crystal structure, not for freestanding, colloidal core-shell semiconductor nanocrystals that are much less stable and easily rotate during examination with an electron beam.

Here, we report how one can measure the atomic structure of a free-standing colloidal core-shell semiconductor nanocrystal with special attention to the interface structure. Our results provide a trustful 3D atomic characterization of the differently oriented interfaces and is applicable to a broad class of technologically important materials, e.g. colloidal hetero-nanocrystals that consist of two different semiconductors but also embedded semiconductor nanostructures that are already used in current technology.

We have studied rod-shaped PbSe(core)-CdSe(shell) hetero-nanocrystals obtained by Cd-for-Pb cation-exchange, starting from PbSe nanocrystal seeds. The experimental details of the synthesis can be found in the supporting information. Revealing the complete atomic structure is essential to gain further understanding of the mechanism of cation exchange at the nanoscale and the chemistry of the PbSe-CdSe interfaces. We remark here that PbSe has a rocksalt crystal structure, whereas the CdSe shell formed by ion-exchange is zincblende. Both phases are cubic with nearly identical lattice parameters, but different atomic coordination: 4-fold coordination in the CdSe zincblende lattice and 6-fold coordination in the PbSe rocksalt lattice. In addition, nanocrystals based on PbSe (and the other Pb chalcogenides) have a band gap in the near-infrared (IR) that can be tailored, due to strong quantum confinement, over a wide spectral region[22]. These systems hold promise for optical and opto-electronic applications[23-25]. By growing a CdSe shell around the PbSe core, the photoluminescence quantum yield increases and the chemical stability improves[26].
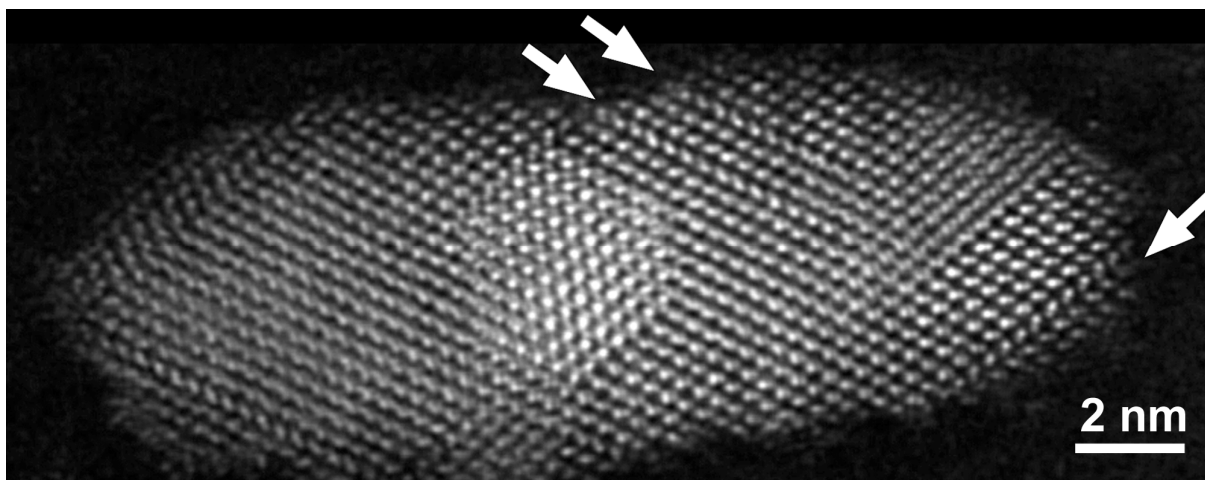
4

Figure 1: HAADF-STEM image of a PbSe-CdSe core-shell structure acquired along the [110] zone axis of PbSe and CdSe. Columns of Pb, Se and Cd can be clearly distinguished. In addition, the Pb columns show clear variations in intensity indicating different numbers of Pb atoms/column. White arrows indicate the presence of stacking faults in the CdSe shell.

Figure 1 shows an example of a PbSe(core)-CdSe(shell) particle imaged along the crystallographic [110] direction using HAADF-STEM. The images were collected using a FEI Titan 50-80 operated at 300kV. The semi-convergence angle used during acquisition was 24 mrad. The core and the shell can be clearly distinguished because of the chemical sensitivity of HAADF-STEM, whereby the intensity is approximately proportional to the square of the atomic number Z. Study of several of these core-shell nanocrystals revealed that the CdSe shell, formed by cation exchange, is always zincblende (for another example, see supporting figure 1) in contrast to colloidal CdSe nanorods obtained by direct synthesis, which have the wurtzite structure[18]. Several stacking faults (indicated by white arrows) are observed. It is likely that these defects result from the process of Cd-for-Pb exchange[27], performed here without further annealing.
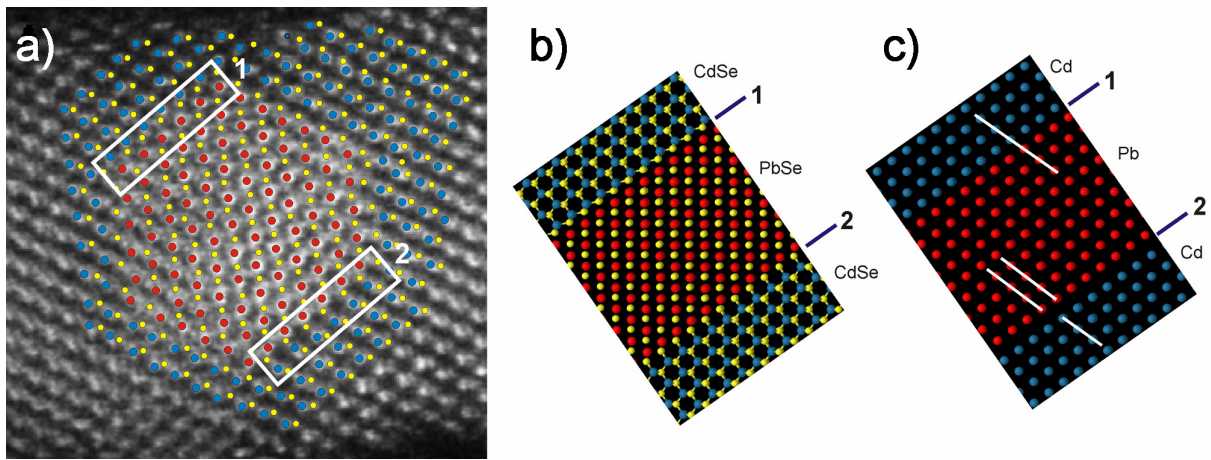
Figure 2: a) Detail of the HAADF-STEM image presented in figure 1, with an atomic overlay where Pb, Cd and Se columns are indicated by red, blue and yellow dots respectively. b) Atomic structure of the PbSe-CdSe interface as obtained from DFT calculations based on the structure displayed in (A). Two different interfaces are present in the periodic supercell. c) Pb, Cd cation sublattice. White lines indicate the lateral alignment of atomic planes across the two interfaces.

The core-shell interfaces are presented in more detail with an atomic overlay in figure 2.a. The position of the Pb, Cd and Se columns are indicated by red, blue and yellow dots, respectively. At the bottom-right interface (marked "2"), it is clear that the Pb and Cd sub-lattices are shifted with respect to each other. Note that the Se sub-lattice remains coherent across the interface. The Pb and Cd sub-lattices display a lateral shift at this interface, which is a natural consequence of the different crystal structures as discussed below. For the nanocrystal displayed in figure 2.a, 3 out of the 4 visible {111} interfacial planes show a shift of the cation sub-lattices in combination with a coherent Se sub-lattice. In contrast, the {111} interface at the top left of the core (marked "1") shows a shift of the Se sub-lattice in combination with coherent Pb/Cd cation sublattices..

The relative atomic positions at both types of interfaces, derived from figure 2.a, are used as input values for an atomistic model of the interface that was relaxed by means of density functional theory (DFT) calculations. These calculations were carried out using the first-principles VASP code[28] employing the projector-augmented wave (PAW) method[29]. The generalized gradient approximation

6

(GGA) digitalized by Perdew, Burke, and Ernzerhof (PBE) was employed for the exchange and correlation energy terms[30]. The configuration used for the calculations is shown in the supporting information (supporting figures 2 and 3), and consists of 9 PbSe {111} bilayers, and 8 CdSe {111} bilayers. Periodic boundary conditions apply, and the supercell thus includes two interfaces. The lattice parameters of the calculation supercell are $a_0=b_0=4.37$ Å, and $c_0=61.97$ Å. It was ascertained that the density of the Monkhorst-Pack k-mesh (Γ-based $16\times16\times1$), and the cutoff energies for the wave functions (300 eV) and augmentation functions (500 eV) were sufficiently high for total energy convergence within 0.5 meV/atom. The cell was allowed to relax both internally (relative atomic positions) and externally (size and shape of the cell). Despite the fact that the initial positions of the atoms were not located at high-symmetry positions, the shape of the supercell always remained hexagonal (with $a_0=b_0$, and $\alpha=60.0°$, $\beta=\gamma=90.0°$) to a high degree of accuracy. The resulting structure, which contains both interfaces, is shown in figure 2.b and 2.c. The inter-atomic forces after relaxation are below 0.01 eV/Å, indicating that both interfaces are mechanically stable. From an analysis of the atomic positions, it follows that the two interfaces are distinctly different. The Se atoms at the top interfacial layer are in a rocksalt type configuration with six nearest neighbors, whereas the Se atoms at the bottom interfacial layer are in a zincblende type configuration with four nearest neighbors. In other words: the interfacial Se atoms at the top interface follow the PbSe lattice, while the interfacial Se atoms at the bottom interface follow the CdSe lattice. It is clear that such results provide unique data for atomistic models of interfaces in colloidal hetero-nanocrystals, and will lead to a better understanding of the physical properties of these systems.

The analysis carried out so far is based on 2D projections of the atomic columns at the interface, in which it was presumed that the interfaces are defect-free and consist of pure Pb or Cd planes. In reality, the absence of Pb and Cd intermixing in the interfacial layer is highly unlikely. In order to gain a more complete 3D understanding of the structure and composition of the interfaces, we have reconstructed the atomic positions of the Pb atoms in the core and at all core-shell interfaces. This is achieved by combining 3 projected images, collected along the [110] (figure 1), the [100] and the [010] zone axis

7

(see supporting figure 4) using HAADF-STEM. In order to determine the number of Pb atoms in the core and interfacial layers, the number of Pb atoms in each projected atomic column is derived from the HAADF-STEM data[21]. The intensities in the HAADF-STEM image have been determined using a model-based approach; they scale with the average atomic number Z and the number of atoms in the column. Next, the statistically meaningful column types with a different number of Pb atoms were determined for the three projection images. The counting results serve as the final input for discrete tomography[31-33], where the following prior knowledge about the core is incorporated: (i) all of the atoms lie on a face-centered-cubic (fcc) grid; (ii) the particle is connected and contains no holes; (iii) the number of edges should be minimized. Using a custom implementation of the simulated annealing algorithm[34], a reconstruction was computed that satisfies these three properties. As the optimization algorithm uses a random number generator, it can be run repeatedly, each time yielding a reconstruction that is possibly different from the previous one. Ten independent reconstructions have been computed, yielding statistics on the fraction of the reconstructions that contains an atom at a certain position; this measure can be interpreted as the certainty about the presence of that particular atom[21].

A comparison between the 3D reconstruction viewed along the original projection directions with the original HAADF-STEM images is presented in supporting figure 5; a good agreement is found. Uncertainties are most likely related to counting errors caused by mistilt of the projection images, collected along the nominal [100] and [010] direction, as the (state-of-the-art) tomography holder used in this study is only able to tilt along one axis. Another factor influencing the counting results is the presence of Cd and Se atoms above and below the PbSe core.
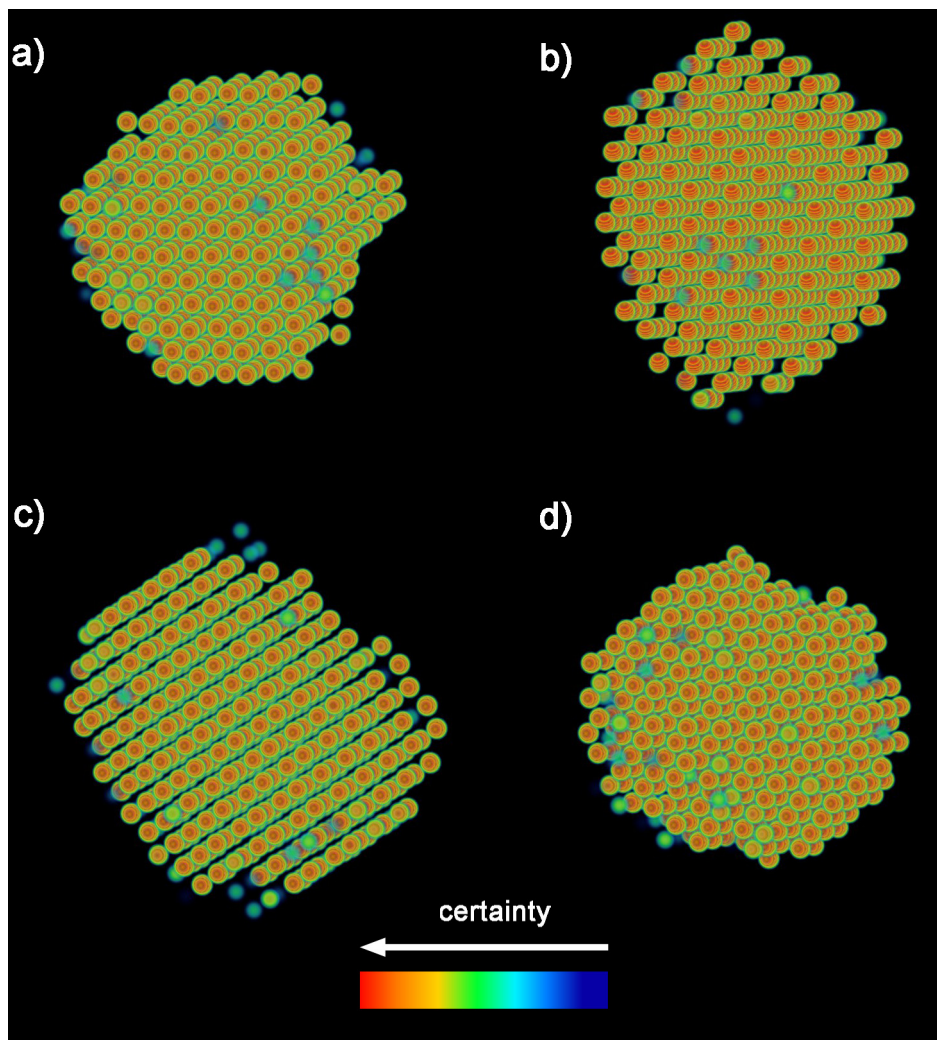
Figure 3: 3D reconstruction of the Pb lattice forming the core of the PbSe-CdSe nanocrystal, along different viewing directions. The color code represents the certainty of the reconstructed atom.

The resulting 3D reconstruction is presented in figure 3, where the reconstructed core of Pb atoms is displayed along different viewing directions. A complete movie is shown in the supporting information. The interfaces of the studied core-shell nanocrystal consist of {111}, {100} as well as {110} planes, which is consistent with a cuboctahedral morphology of the core. From figures 1 and 3, it is clear that the boundary between the PbSe core and the CdSe shell is very sharp, indicating that the diffusion of the Pb ions, that must leave the core-shell structure through the CdSe shell, is a fast process. The details of the 3D reconstruction reveal that several interfacial planes are found to be incomplete regarding the occupancy of Pb atoms (see, e.g., the 'island' of Pb atoms at the right-hand side of the core in figure 3.a) and therefore consist of a mixture of Pb and Cd atoms. These results show that ion-exchange

possibly proceeds in a layer by layer fashion along certain crystallographic planes, replacing Pb by Cd. If this would not be the case, there would be a large volume in which Pb and Cd atoms are intermixed, in clear contrast to our 3D results. From the position of the PbSe core in the elongated CdSe structure it is clear that Pb for Cd cation exchange constitutes a highly anisotropic process. Indeed, if the reaction mechanism would be fully isotropic, one would expect a rod-in-rod configuration, in contrast to our results. However, the central position of the core implies that the cation exchange reaction proceeded with the same speed from the opposite facets of the initial nanocrystal, whereby different types of facets ({111}, {110}, {100}) have different reaction speeds.

In summary, we have characterized the atomic configuration of a free-standing colloidal hetero-nanocrystal using a combination of HAADF-STEM projections and discrete tomography. The interfaces show mostly a coherency in the Se-sublattice and interfacial mixing of Pb and Cd atoms. Our results, which are obtained on a free-standing particle consisting of semiconductor compounds, provide essential insights into the cation exchange mechanism which is widely used in the synthesis of colloidal hetero-nanocrystals. On a more general note, 3D results such as presented in this study can provide more realistic structural input for theoretical modelling of nanoscale interfaces, leading to a better insight on the relationship between the structure and properties of semiconductor hetero-structures and miniaturized devices.

SUPPORTING INFORMATION PARAGRAPH

A movie of the 3D reconstruction can be found as supporting information as well as synthesis details, additional images of the core-shell particles and the supercell used for DFT calculations.

REFERENCES

(1)   Hines, M. A.; Guyot-Sionnest, P. Synthesis and Characterization of Strongly Luminescing ZnS-Capped CdSe Nanocrystals. *J. Phys.Chem.* **1996**, *100*, 468-471.

(2)   Dabbousi, B. O.; Rodriguez-Viejo, J.; Mikulec, F.V.; Heine, J.R.; Mattoussi, H.; Ober, R.; Jensen, K.F.; Bawendi, M.G. (CdSe)ZnS Core−Shell Quantum Dots: Synthesis and Characterization of a Size Series of Highly Luminescent Nanocrystallites. J. Phys.Chem. B **1997**, *101*, 9463-9475.

(3)   Peng, X. G.; Schlamp, M. C.; Kadavanich, A. V.; Alivisatos, A. P. Epitaxial Growth of Highly Luminescent CdSe/CdS Core/Shell Nanocrystals with Photostability and Electronic Accessibility *J. Am. Chem. Soc.* **1997***, 119*, 7019-7029.

(4)   Reiss, P.; Bleuse, J.; Pron, A. Highly Luminescent CdSe/ZnSe Core/Shell Nanocrystals of Low Size Dispersion. *Nano Lett.* **2002**, *2*, 781-784.

(5)   Mahler, B.; Spinicelli, P.; Buil, S.; Quelin, X.; Hermier, J.-P.; Dubertret, B. Towards non-blinking colloidal quantum dots. *Nat. Mater.* **2008**, *7*, 659-664.

(6)   Wang, X.Y.; Ren, X.; Kahen, K.; Hahn, M.A.; Rajeswaran, M.; Maccagnano-Zacher, S.; Silcox, J.; Gragg, G.E.; Efros, A.L.; Krauss, T. D.; Non-blinking semiconductor nanocrystals. *Nature* **2009**, *459,* 686-689.

(7)   Dubertret, B.; Skourides, P.; Norris, D.J.; Noireaux, V.; Brivanlou, A.H.; Lichaber, A.; In Vivo Imaging of Quantum Dots Encapsulated in Phospholipid Micelles. *Science* **2002**, *298*, 1759-1762.

(8)   Amirav, L.; Alivisatos, A. P. Photocatalytic Hydrogen Production with Tunable Nanorod Heterostructures. *J. Phys.Chem. Lett.* **2010**, *1*, 1051-1054.

(9)   Ziegler, J.; Xu, S.; Kucur, E.; Meister, F.; Batentschuk, M.; Gindele, F.; Nann, T. Silica-Coated InP/ZnS Nanocrystals as Converter Material in White LEDs. *Adv. Mater.* **2008**, *20*, 4068-4073.

(10)   Klimov, V. I.; Mikhailovsky, A.A.; Xu, S.; Malko, A.; Hollingsworth, J.A.; Leatherdale, C.A.; Eisler, H.-J.; Bawendi, M.G.. Optical Gain and Stimulated Emission in Nanocrystal Quantum Dots. *Science* **2000**, *290*, 314-317.

(11)   Li, J. J.; Tsay, J. M.; Michalet, X.; Weiss, S. Wave-function engineering: from quantum wells to near-infrared type-II colloidal quantum dots synthesized by layer-by-layer colloidal epitaxy. *Chem. Phys.* **2005**, *318*, 82-90.

(12)   Xie, R.; Zhong, X.; T. Basché Synthesis, Characterization, and Spectroscopy of Type-II Core/Shell Semiconductor Nanocrystals with ZnTe Cores. *Adv. Mater.* **2005**, *17*, 2741-2745.

(13)   Chin, P.T.K.; de Mello Donegá, C.; van Bavel, S.S.; Meskers, S.C.J.; Sommerdijk, N.A.J.M.; Janssen, R.A.J. Highly Luminescent CdTe/CdSe Colloidal Heteronanocrystals with Temperature-Dependent Emission Color. *J. Am. Chem. Soc.* **2007**, *129*, 14880-14886.

(14)   Steiner, D.; Dorfs, D.; Banin, U., Della Sala, F.; Manna, L.; Millo, O. Determination of Band Offsets in Heterostructured Colloidal Nanorods Using Scanning Tunneling Spectroscopy. *Nano Lett.* **2008**, *8*, 2954-2958.

(15)   Osovsky, R.; Cheskis, D.; Kloper, V.; Sashchiuk, A.; Kroner, M.; Lifshitz, E. Continuous-Wave Pumping of Multiexciton Bands in the Photoluminescence Spectrum of a Single CdTe-CdSe Core-Shell Colloidal Quantum Dot. *Phys. Rev. Lett.* **2009**, *102*, 197401.

(16) Htoon, H.; Malko, A.V.; Bussian, D.; Vela, J.; Chen, Y.; Hollingsworth, J.; Klimov, V.I. Highly Emissive Multiexcitons in Steady-State Photoluminescence of Individual "Giant" CdSe/CdS Core/Shell Nanocrystals. *Nano Lett.* **2010**, *10*, 2401-2407.

(17) Klimov, V. I.; Ivanov, S.; Nanda, J.; Achermann, M.; Bezel, I.; McGuire, J.A.; Piryatinski, A. Single-exciton optical gain in semiconductor nanocrystals. *Nature* **2007**, *447*, 441-446.

(18) Manna, L.; Scher, E. C.; Li, L. S.; Alivisatos, A. P. Epitaxial growth and photochemical annealing of graded CdS/ZnS shells on colloidal CdSe nanorods. *J. Am. Chem. Soc.* **2002**, *124*, 7136-7145.

(19) Talapin, D. V.; Mekis, I.; Götzinger, S.; Kornowski, A.; Benson, O.; Weller, H. CdSe/CdS/ZnS and CdSe/ZnSe/ZnS Core−Shell−Shell Nanocrystals. *J. Phys.Chem. B* **2004**, *108*, 18826-18831.

(20) Mattila, T.; Wang, L. W.; Zunger, A. Electronic consequences of lateral composition modulation in semiconductor alloys. *Phys. Rev.B* **1999**, *59*, 15270-15284.

(21) Van Aert, S.; Batenburg, K. J.; Rossell, M. D.; Erni, R.; Van Tendeloo, G. Three-dimensional atomic imaging of crystalline nanoparticles. *Nature* **2011**, *470*, 374-377.

(22) Wise, F. W. Lead Salt Quantum Dots: the Limit of Strong Quantum Confinement. *Acc. Chem. Res.* **2000**, *33*, 773-780.

(23) Konstantatos, G.; Howard, I.; Fischer, A.; Hoogland, S.; Clifford, J.; Klem, E.; Levina, L.; Sargent, H.S. Ultrasensitive solution-cast quantum dot photodetectors. *Nature* **2006,** *442*, 180-183.

(24) Wang, R. Y.; Feser, J.P.; Lee, J.-S.; Talapin, D.V.; Segalman, R.; Majumdar, A. Enhanced Thermopower in PbSe Nanocrystal Quantum Dot Superlattices. *Nano Lett.* **2008,** *8*, 2283-2288.

(25) Nozik, A. J. Nanoscience and Nanostructures for Photovoltaics and Solar Fuels. *Nano Lett.* **2010,** *10*, 2735-2741.

(26) Pietryga, J. M.; Werder, D.J.; Williams, D.J.; Casson, J.L.; Scaller, R.D.; Klimov, V.I.; Hollingsworth, J.A. Utilizing the Lability of Lead Selenide to Produce Heterostructured Nanocrystals with Bright, Stable Infrared Emission. *J. Am. Chem. Soc.* **2008**, *130*, 4879-4885.

(27) Lambert, K.; Geyter, B. D.; Moreels, I.; Hens, Z. PbTe|CdTe core|shell particles by cation exchange, a HR-TEM study. *Chem.Mater.* **2009**, *21*, 778-780.

(28) Kresse, G.; Furthmüller, J. Efficiency of ab-initio total energy calculations for metals and semiconductors using a plane-wave basis set. *Comput. Mater. Sci.* **1996**, *6*, 15-50.

(29) Kresse, G.; Furthmüller, J., Efficient iterative schemes for ab-initio total energy calculations using a plane-wave basis set. *Phys. Rev. B* **1996**, *54*, 11169.

(30) Perdew, J. P.; Burke, K.; Ernzerhof, M. Generalized Gradient Approximation Made Simple. *Phys. Rev. Lett.* **1996,** *77*, 3865.

(31) Jinschek, J.R.; Batenburg, K.J; Calderon, H.A.; Kilaas, R.; Radmilovic, V.; Kisielowski, C. 3-D reconstruction of the atomic positions in a simulated gold nanocrystal based on discrete tomography: Prospects of atomic resolution electron tomography. *Ultramicroscopy*, **2008**, *108*, 589-604.

(32) Bals, S.; Batenburg, K. J.; Verbeeck, J.; Sijbers, J.; Van Tendeloo, G. Quantitative Three-Dimensional Reconstruction of Catalyst Particles for Bamboo-like Carbon Nanotubes. *Nano Lett.* **2007**, *7*, 3669-3674.

(33) Batenburg, K. J.; Bals, S.; Sijbers, J.; Kübel, C.; Midgley, P.A.; Hernandez, J.C; Kaiser, U.; Encina, E.R.; Coronado, E.C.; Van Tendeloo, G. 3D imaging of nanomaterials by discrete tomography. *Ultramicroscopy,* **2009**, *109*, 730-740.

(34) Kirkpatrick, S.; Gelatt, C.D.; Vecchi, M.P. Optimization by simulated annealing. *Science* **1983**, *220***,** 671-680.

SYNOPSIS TOC